Influence of the disposition of the anisotropy axis into the magnetic properties of dinuclear Mn$_{III}$ compounds with benzoato derivative bridges

Beltzane Garcia-Cirera[a], Silvia Gómez-Coca[a,c]*†, Mercè Font-Bardia[b], Eliseo Ruiz[a,c],

Montserrat Corbella[a,d]*

[a]Departament de Química Inorgànica i Orgànica, Universitat de Barcelona, Barcelona, Spain.

[b]Cristal·lografia, Mineralogia i Dipòsits Minerals, Universitat de Barcelona, Barcelona, Spain.

[c]Institut de Química Teórica i Computacional de la Universitat de Barcelona (IQTCUB), Barcelona, Spain.

[d]Institut de Nanociencia i Nanotecnologia de la Universitat de Barcelona (IN2UB), Barcelona, Spain.

ABSTRACT

Two new dinuclear Mn$_{III}$ compounds [{Mn(phen)(H$_2$O)}$_2$(μ-4-CH$_3$C$_6$H$_4$COO)$_2$(μ-O)](ClO$_4$)$_2$·3CH$_3$CN·H$_2$O (**1**·3CH$_3$CN·H$_2$O) and [{Mn(phen)(H$_2$O)}(μ-O)(μ-2-BrC$_6$H$_4$COO)$_2${Mn(phen)(NO$_3$)}]NO$_3$ (**2**) have been synthetized. Their structural data reveals

significant differences in the shape of the coordination octahedron around the Mn_{III} ions in both compounds. The different distortion from the ideal octahedron incite a very different magnetic behavior, affecting both, the zero-field splitting parameters of the Mn_{III} ions (D_{Mn} and E_{Mn}) and the magnetic interaction between them. Compound **1**, with elongated coordination octahedra, in the monodentate ligand direction, shows a ground state $S = 0$ and $D_{Mn} < 0$, while compound **2** with compressed coordination octahedra, in the oxo bridge direction, shows a ground state $S = 4$ and $D_{Mn} > 0$. Theoretical CASSCF and DFT calculations corroborate the different magnetic anisotropy and exchange coupling founded in both compounds. Moreover, with the help of theoretical calculations, some interesting magneto-structural correlations have been found between the degree of distortion of the coordination octahedra and the magnetic coupling, it becomes more antiferromagnetic when the elongation parameter, Δ, in absolute value is increased.

INTRODUCTION

The magnetic properties of the dinuclear Mn_{III} compounds with the core $[Mn_2(\mu\text{-}O)(\mu\text{-}R'COO)_2]_{2+}$ have been widely studied; the electronic configuration of the Mn_{III} ions (d_4) with an empty d orbital is the responsible of the weak magnetic interaction between the Mn_{III} ions and the magnetic behavior could be ferro- or antiferromagnetic.[1] Several structural parameters influence the kind and degree of this interaction. The most important factor is the shape of the coordination octahedron, due to the Jahn-Teller effect. It was observed that compounds with tridentate blocking ligands show compressed octahedra around the Mn_{III} ions, with the short distortion axis pointing to the oxo bridging ligand. When the capping ligand is bidentate, the sixth position is occupied by a monodentate ligand and this fact provides a major flexibility to the coordination octahedra.[2] Compounds with general formula $[\{Mn(NN)(L)\}_2(\mu\text{-}O)(\mu\text{-}n\text{-}RC_6H_4COO)_2]_{n+}$ usually shows elongation of the octahedra in the direction of the monodentate

ligand.[3–9] There is only one compound reported in the literature with compressed octahedral around the Mn_{III} ions, [{Mn(bpy)(N$_3$)}$_2$(μ-O)(μ-C$_6$H$_5$COO)$_2$], which shows an important ferromagnetic coupling.[10,11]

In last years, we have focused our attention to found the structural parameters that control the magnetic behavior, and consequently the ground state of the system, $S = 0$ or $S = 4$.[4–7,12] Recently we reported the influence of the anisotropy of the Mn_{III} ions and the orientation of the distortion axis on the magnetic behavior at low temperature.[9]

The magnetic anisotropy provided by the Mn_{III} ions is quantified by the axial zero field splitting (ZFS) parameter, D_{Mn}, which depends on the spin-orbit coupling. The magnetic anisotropy of Mn ions have been widely studied in the last years because this ion was proposed as source of magnetic anisotropy due to its presence in several polynuclear single molecule magnets (SMM).

To further understand its magnetic anisotropy several theoretical studies have been devoted to mononuclear Mn compounds,[13] including a systematic study of the magnetic anisotropy of mononuclear Mn_{III} complexes.[14] For these complexes the D_{Mn} values ranges between -5 and +4 cm$_{-1}$, being negative for elongated systems and positive for compressed systems, and showing that both usually employed approaches to calculate ZFS parameters (DFT and CASSCF) reproduce remarkably well the experimental values.[13,14]

Regarding the theoretical study of the magnetic anisotropy of dinuclear Mn_{III} compounds, it is worth noting the study of the [{Mn(L')}$_2$(μ-O)(μ-OAc)$_2$](PF$_6$)$_2$ (with a tridentate capping ligand L' = trispyrrolidine-1,4,7-triazacyclononane) compound, in which the Mn_{III} is in a compressed octahedral environment and shows a ferromagnetic coupling and a positive D value.[15] Simulation changing structural parameters showed that the coupling constant is highly sensitive to small structural variations becoming antiferromagnetic for shorter Mn–O$_{oxo}$ distance and larger Mn–O$_{oxo}$–Mn angle. In their model calculations it becomes

antiferromagnetic for a Mn–O_{oxo}–Mn angle of 123.91º and an Mn–O_{oxo} distance equal to 1.798 Å.[15]

In this work we report the synthesis, crystal structure and magnetic study of two new dinuclear Mn_{III} compounds [{Mn(phen)(H_2O)}$_2$(μ-4-$CH_3C_6H_4COO$)$_2$(μ-O)](ClO_4)$_2$· 3CH_3CN·H_2O (1·3CH_3CN·H_2O) and [{Mn(phen)(H_2O)}(μ-O)(μ-2-BrC_6H_4COO)$_2${Mn(phen)(NO_3)}]NO_3 (2). The structural data reveals significant differences in the shape of the coordination octahedra of both compounds. We have performed combined experimental and theoretical studies to analyze the magnetic properties of these compounds, being our goal in this manuscript to understand and rationalize the effect of the orientation of the Jahn-Teller axis on the magnetic behavior.

EXPERIMENTAL SECTION

Synthesis. All manipulations were carried out at room temperature under aerobic conditions. Reagents and solvents were obtained from commercial sources and used without further purification. NBu_4MnO_4 was prepared as described in the literature.[16] Yields were calculated from stoichiometric reaction. Caution! *Perchlorate salts of compounds containing organic ligands are potentially explosive. Only small quantities of these compounds should be prepared and handled behind suitable protective shields.*

[{Mn(phen)(H_2O)}$_2$(μ-4-$CH_3C_6H_4COO$)$_2$(μ-O)](ClO_4)$_2$· 3CH_3CN·H_2O (1·3CH_3CN·H_2O)

4-$CH_3C_6H_4COOH$ (0.22 g, 1.62 mmol) and Mn(ClO_4)$_2$·6H_2O (0.45 g, 1.24 mmol) were solved in 15 mL of CH_3CN. Then, 10 mL of NBu_4MnO_4 (0.11 g, 0.32 mmol) solution and 5 mL of 1,10-phenantroline·H_2O (phen) (0.29 g, 1.46 mmol), both in CH_3CN, were added at the same time in the above-mentioned solution and immediately turned in dark-brown. The mixture was

stirred for 15 min and any precipitate was formed. The solution was left undisturbed in the refrigerator. One month later dark brown crystals suitable for X-ray diffraction were obtained. The product was separated by filtration. Yield: 27%. Anal. Calcd for $Mn_2C_{40}H_{34}N_4O_{15}Cl_2 \cdot 0.5$ H_2O (M.W. = 1000.51) (%): C, 48.01; H, 3.52; N, 5.60. Found: C, 47.90; H, 3.56; N, 5.65. Selected IR data (KBr, main bands, cm$_{-1}$): 3457(m), 3065(w), 1608(m), 1629(w), 1590(s), 1550(s), 1518(vs), 1427(s), 1385(vs), 1374(vs), 1341(s), 1110(vs), 849(s), 762(s), 721(s), 624(s).

[{Mn(phen)(H$_2$O)}(μ-O)(μ-2-BrC$_6$H$_4$COO)$_2${Mn(phen)(NO$_3$)}]NO$_3$ (2)

2-BrC$_6$H$_4$COOH (0.13 g, 0.65 mmol) and Mn(NO$_3$)$_2$·xH$_2$O (0.10 g, 0.56 mmol) were solved in 5 mL of CH$_3$CN. Then, 5mL of NBu$_4$MnO$_4$ (0.03 g, 0.08 mmol) solution and 5 mL of 1,10-phenantroline·H$_2$O (phen) (0.13 g, 0.66 mmol), both in CH$_3$CN, were added at the same time in the above-mentioned solution and some precipitate was formed. The mixture was heated in a microwave devise from 25 ºC to 85 ºC in 12 min. The final temperature was maintained for 5 min and then, the mixture was slowly cooled down until 25 ºC. The obtained microcrystalline powder was removed by filtration and the mother solution was left undisturbed at room temperature. After few days, dark brown crystals suitable for X-ray diffraction were obtained. Yield: 45%. Anal. Calcd for $Mn_2C_{38}H_{26}N_6O_{12}Br_2$ (1028.33) (%): C, 44.38; H, 2.55; N, 8.17. Found: C, 44.21; H, 2.51; N, 8.01. Selected IR data (KBr, main bands, cm$_{-1}$): 3433(m), 1627(w), 1594(s), 1561(w), 1518(w), 1426(s), 1384(vs), 1104(w), 1022(s), 873(w), 844(m), 755(m), 718(s).

Physical measurements and instruments

The synthesis of compound **2** was carried out in an Anton Paar Monowave 300 Synthesis Reactor. Chemical analyses of C, H, N were carried out by the "Servei de Microanàlisi" of the "Consell Superior d'Investigacions Científiques (CSIC)". Infrared spectra

were recorded on KBr pellets in the 4000 – 400 cm^{-1} range with a Thermo Nicolet Avatar 330 FT - IR spectrometer. Magnetic susceptibility (χ_M) measurements between 2 – 300 K were carried out in a Quantum Design MPMS XL5 SQUID Magnetometer at the "Unitat de Mesures Magnètiques (Universitat de Barcelona)", using a field of 200 G. Pascal's constants were used to estimate the diamagnetic corrections for each compound. Magnetization measurements ($M/N\mu_\beta$), were carried out in the range 1.8 – 6.8 K and at six different magnetic fields (0.5, 1.0, 2.0, 3.0, 4.0 and 5.0 T). The accuracy of the fit was calculated by the functions $R_{sus} = \Sigma[(\chi_M T)_{exp} - (\chi_M T)_{calc}]^2/\Sigma[(\chi_M T)_{exp}]^2$ and $R_{mag} = \Sigma[(M/N\mu_\beta)_{exp} - (M/N\mu_\beta)_{calc}]^2/\Sigma[(M/N\mu_\beta)_{exp}]^2$.

Crystallographic Data Collection and Refinement

X-ray crystallographic data for crystals of **1** and **2** were collected at 100 K. Compound **1** was mounted on a MAR345 diffractometer with an image plate detector and compound **2** on a D8 Venture system equipped with a Multilayer monochromator. For compounds **1** and **2** the structure was solved by Direct methods, using SHELXS computer program and refined by full-matrix least-squares method with SHELX97 computer program.[17] All H atoms were computed and refined, using a riding model with an isotropic temperature factor equal to 1.2 time the equivalent temperature factor of the atom which are linked. Crystal data collection and refinement parameters are given in Table 1.

Table 1. X-ray Crystallographic Data for compounds **1** and **2**

	1·3CH₃CN·H₂O	**2**
chemical formula	$C_{46}H_{45}Cl_2Mn_2N_7O_{16}$	$C_{38}H_{26}Br_2Mn_2N_6O_{12}$
formula weight /g mol^{-1}	1132.67	1028.35
T / K	100(2)	104(2)
λ (Mo Kα) / Å	0.71073	0.71073
crystal system	$P\bar{1}$	Pna21
space group	Triclinic	Orthorhombic
crystal size / mm	0.1 x 0.09 x 0.08	0.74 x 0.17 x 0.126
A / Å	11.734(5)	18.0696(5)
B / Å	12.925(4)	20.3810(5)
C / Å	18.325(6)	10.5036(3) Å
α / deg.	91.91(2)	90
β / deg.	108.60(2)	90
χ / deg.	103.83(2)	90
V / Å³	2539.5(16)	3868.23(18)
Z	2	4
ρ$_{calcd}$ / g cm^{-3}	1.481	1.766
μ / mm^{-1}	0.678	2.792
F(000)	1164	2048
Θ range / deg.	1.63 to 32.29	2.181 to 30.044
limiting indices	h =-14→16, k = -18→15, l = -26→26	h = -25→25, k = -28→28, l = -14→12
data / restraints / parameters	12500 / 9 / 771	10651 / 5 / 517
goodness-of-fit on F₂	1.087	1.028
final R indices [I>2σ(I)]	R1 = 0.0626, wR2 = 0.1729	R1 = 0.0477, wR2 = 0.1136
R indices (all data)	R1 = 0.0786, wR2 = 0.1837	R1 = 0.0613, wR2 = 0.1217

Compound 1: A prism-like specimen of $C_{46}H_{45}Cl_2Mn_2N_7O_{16}$, approximate dimensions 0.080 mm x 0.090 mm x 0.100 mm, was used for the X-ray crystallographic analysis. The X-ray intensity data were measured on a MAR345 system equipped with a graphite monochromator and a Mo fine-focus sealed tube (λ = 0.71073 Å). The frames were integrated with the Bruker SAINT software package using a MARSCALE algorithm. The integration of the data using a triclinic unit cell yielded a total of 22266 reflections to a maximum θ angle of 32.29° (0.67 Å resolution), of which 12500 were independent (average redundancy 1.781,

completeness = 69.2 %, Rint = 3.96 %, Rsig = 4.24 %) and 9675 (77.40 %) were greater than $2\sigma(F2)$. The final cell constants of a = 11.734(5) Å, b = 12.925(4) Å, c = 18.325(6) Å, α = 91.91(2)°, β = 108.60(2)°, γ = 103.83(2)°, volume = 2539.5(16) Å3, are based upon the refinement of the XYZ-centroids of reflections above 20 $\sigma(I)$. Data were corrected for absorption effects using the empirical method (SADABS). The calculated minimum and maximum transmission coefficients (based on crystal size) are 0.5000 and 0.5000. The structure was solved and refined using the Bruker SHELXTL Software Package, using the space group P -1, with Z = 2 for the formula unit, $C_{46}H_{45}Cl_2Mn_2N_7O_{16}$. The final anisotropic full-matrix least-squares refinement on F2 with 771 variables converged at R1 = 6.26 %, for the observed data and wR2 = 18.37 % for all data. The goodness-of-fit was 1.087. The largest peak in the final difference electron density synthesis was 2.403 e- Å-3 and the largest hole was -0.647 e- Å-3 with an RMS deviation of 0.075 e- Å-3. On the basis of the final model, the calculated density was 1.481 g cm-3 and F(000), 1164 e-.

Compound 2: A red prism-like specimen of $C_{38}H_{26}Br_2Mn_2N_6O_{12}$, approximate dimensions 0.126 mm x 0.170 mm x 0.520 mm, was used for the X-ray crystallographic analysis. The X-ray intensity data were measured on a D8 Venture system equipped with a multilayer monochromator and a Mo microfocus (λ = 0.71073 Å). The frames were integrated with the Bruker SAINT software package using a narrow-frame algorithm. The integration of the data using an orthorhombic unit cell yielded a total of 84643 reflections to a maximum θ angle of 30.04° (0.71 Å resolution), of which 10651 were independent (average redundancy 7.947, completeness = 99.5 %, Rint = 6.00 %, Rsig = 4.55 %) and 9096 (85.40 %) were greater than $2\sigma(F2)$. The final cell constants of a = 18.0696(5) Å, b = 20.3810(5) Å, c = 10.5036(3) Å, volume = 3868.23(18) Å3, are based upon the refinement of the XYZ-centroids of reflections above 20 $\sigma(I)$. Data were corrected for absorption effects using the psi-scan method (SADABS). The structure was solved using the Bruker SHELXTL Software Package, and

refined using SHELXL,[17] using the space group P n a 21, with Z = 4 for the formula unit, $C_{38}H_{26}Br_2Mn_2N_6O_{12}$. The final anisotropic full-matrix least-squares refinement on F2 with 517 variables converged at R1 = 4.77 %, for the observed data and wR2 = 12.17 % for all data. The goodness-of-fit was 1.028. The largest peak in the final difference electron density synthesis was 2.829 e- Å-3 and the largest hole was -1.710 e- Å-3 with an RMS deviation of 0.127 e- Å-3. On the basis of the final model, the calculated density was 1.766 g/cm3 and F(000), 2048 e-.

Computational Details

Due to the strong dependence of the magnetic coupling constant and ZFS parameters with small structural changes all the calculations were performed using the crystallographic geometries obtained by X-ray diffraction.

The calculation of the ZFS parameters have been performed with the MOLCAS code (version 7.8)[18] using the procedure described by Maurice et al,[19] that consist in performing a CASSCF calculation first, followed by the mixing of the energy of these CASSCF states within the SO-RASSI approach. After that, the axial (D_{Mn}) and rhombic (E_{Mn}) ZFS parameters together with the *g* and **D** tensors were extracted using the Single-Aniso software.[20] The calculation of the magnetic anisotropy of each MnIII ions has been done using the geometry of the whole complex but replacing one of the MnIII ions for a GaIII ion. This procedure was done for both sites of the dinuclear entity. The electronic configuration of MnIII is d_4, so the selected active space CAS(4,5) contains 4 electrons in the 5 essentially atomic *d* orbitals. All the quintet, triplet and singlet states were included in the calculations.

For the evaluation of the magnetic coupling constant of the dinuclear MnIII systems, the employed methodology has been previously described by Ruiz et al.[21–23] The calculations were carried out using the density functional theory (DFT) with the Gaussian09 software (version g09d01),[24] the hybrid B3LYP functional[25] and the triple-ζ basis set proposed by Schaefer et. al.[26] The initial wave function was generated previously with the Jaguar software (version

7.5)[27] including the effects of the ligands field.[28] Two spin distributions have been calculated for the Mn$_{III}$ dinuclear system, the high spin one ($S_T = 4$), in which the spin in both Mn ions are parallel, and the low spin one ($S_T = 0$), where the spin of Mn2 is reversed. The exchange coupling constant has been obtained from the energy difference between the two spin distributions ($E_{ls} - E_{hs} = 10J$).

The influence of the structural parameters has been analyzed by the construction of three kind of models based on the crystal structures of **1** and **2**: a) The angle formed by the Mn ions and oxo bridge (Mn-O$_b$-Mn) have been modified in the 120-125° range; this variation provokes a slight change in the Mn-O$_b$ distances (Tables S1 and S2). b) The Mn-L distance, being L the monodentate ligand, have been varied in the 2.1-2.3 Å range (Tables S3 and S4). And c) the Mn-N$_t$ distances, where N$_t$ is the nitrogen atom trans to the oxo bridge, have been modified between 2.025 and 2.1 Å; the shift of the N$_t$ atoms shift also the other nitrogen atom, N$_c$, of the ligand (Tables S5 and S6).

RESULTS AND DISCUSSION

Synthesis

These dinuclear Mn$_{III}$ compounds were obtained by a comproportionation reaction between MnX$_2$ (X = ClO$_4$ (**1**) or NO$_3$ (**2**)) and Bu$_4$NMnO$_4$, in the presence of the carboxylic acid (4-MeC$_6$H$_4$COOH for **1** and 2-BrC$_6$H$_4$COOH for **2**) and 1,10-phenanthroline leading to compounds with general formula [{Mn(L)(phen)}(μ-n-RC$_6$H$_4$COO)$_2$(μ-O){Mn(L')(phen)}]X$_{2-m}$. L and L' are monodentate ligands that can be H$_2$O or X. For compound **1** L and L' are H$_2$O molecules, while for **2**, one of the monodentate positions is occupied by the nitrate anion; so compound **1** shows a divalent cation while **2** a monovalent cation.

The synthesis of compound **2** by the traditional method was unsuccessful due to the formation of sub-products and the low crystallinity of the desired compound. So, the reaction was performed heating the sample above the boiling point of the solvent, in a microwave device, on a closed vessel.

The infrared spectra of these compounds show two characteristic bands of the carboxylate ligand at ~1600 and ~1380 cm^{-1}, corresponding to the asymmetric and symmetric vibrations, respectively. The values of $\Delta v = v_a(COO) - v_s(COO)$, being ~200 cm^{-1}, are indicative of carboxylate ligands coordinated in a bidentate bridging mode ($\mu_{1,3}$).[29] The nitrate anions show a very strong band at ~1384 cm^{-1}, which appears overlapped with the carboxylate one. The perchlorate anions display broad bands at ~1100 cm^{-1} and a band of moderate intensity at 623 cm^{-1}. Bidentate phen ligands show characteristic bands in the 1600–1400 cm^{-1} and 850–600 cm^{-1} regions. The Mn–O$_b$–Mn group usually displays a band at ~730 cm^{-1}, but is masked by 1,10-phenanthroline bands.

Description of Structures.

The crystal structures of compounds **1** [{Mn(H$_2$O)(phen)}$_2$(μ-4-CH$_3$C$_6$H$_4$COO)$_2$(μ-O)](ClO$_4$)$_2$·3CH$_3$CN·H$_2$O and **2** [{Mn(H$_2$O)(phen)}(μ-2-BrC$_6$H$_4$COO)$_2$(μ-O){Mn(NO$_3$)(phen)}]NO$_3$ are shown in Figure 1. In both compounds the two Mn$_{III}$ ions are bridged by one oxo and two $\mu_{1,3}$-n-RC$_6$H$_5$COO$_-$ ligands (n-R = 4-Me for **1** and 2-Br for **2**). Each manganese ion is chelated by a 1,10-phenanthroline (phen) ligand and the hexacoordination is completed by a monodentate ligand. In compound **1** the monodentate ligands are water molecules, while in compound **2** one of the monodentate ligands is a nitrate anion and the other one is a water molecule.
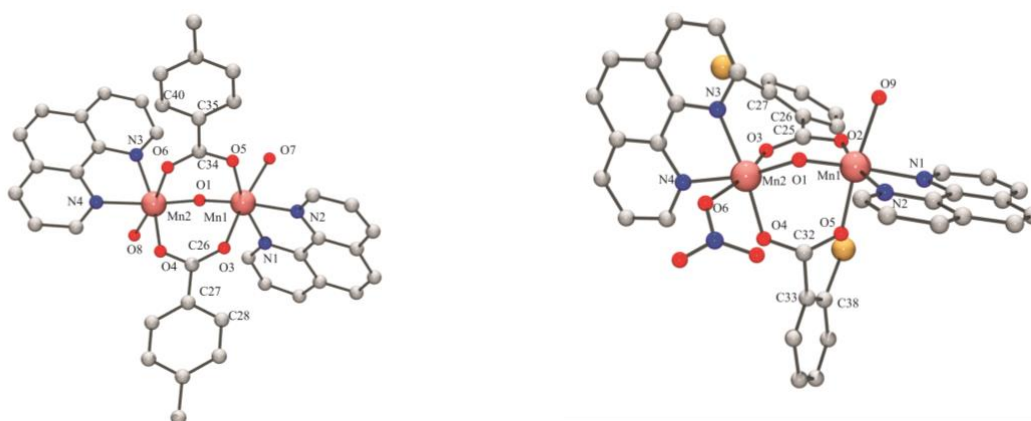
Figure 1. Crystal structures of the cationic complexes of compounds **1** (left) and **2** (right). Hydrogen atoms are omitted for clarity.

The structural parameters of these compounds are in agreement with those reported for analogous compounds with the same $[Mn_2(\mu\text{-}O)(\mu\text{-}RC_6H_5COO)_2]^{2+}$ core.[2,4–6,9,11,12,30–32] Selected bond lengths and angles are listed in Table 2. The Mn···Mn distance is ~3.14 Å and the Mn–O–Mn angle is ~123°. The Mn–O bond lengths of the oxo bridge are ~1.79 Å and the Mn–N distances ~2.09 Å.

The carboxylate bridging ligands are coordinated in a *syn-syn* conformation mode. One of the oxygen atoms is placed *trans* to the monodentate ligand, with Mn–O_t distance of ~2.15 Å for **1** and ~2.13 Å for **2**, whereas the other oxygen atom is placed in a *cis* position with a shorter Mn–O_c distance (~1.96 Å for **1** and ~2.01 Å for **2**). A significant difference between these compounds can be found in the Mn–O_L bond lengths: for compound **1,** the Mn–O_w distances are 2.233 and 2.198 Å, whereas for compound **2** the Mn–O_w distance is 2.130 Å and the Mn–O_{NO3} distance is 2.164 Å.

Table 2. Selected bond lengths (Å) and angles (deg.) for compounds **1·3CH₃CN·H₂O** and **2**.

1·3CH$_3$CN·H$_2$O		2	
Mn(1)-O(1)	1.803(2)	Mn1-O1	1.778(4)
Mn(1)-N(2)	2.082(2)	Mn1-N1	2.086(4)
Mn(1)-O(5)	1.967(2)	Mn1-O2	2.028(4)
Mn(1)-N(1)	2.095(3)	Mn1-N2	2.127(5)
Mn(1)-O(3)	2.1505(19)	Mn1-O5	2.105(5)
Mn(1)-O(7)	2.233(2)	Mn1-O9	2.130(4)
Mn(1)···Mn(2)	3.136(1)	Mn1···Mn2	3.1419(10)
Mn(2)-O(1)	1.779(2)	Mn2-O1	1.777(4)
Mn(2)-N(4)	2.073(3)	Mn2-N4	2.071(4)
Mn(2)-O(4)	1.952(2)	Mn2-O4	1.999(4)
Mn(2)-N(3)	2.097(3)	Mn2-N3	2.093(5)
Mn(2)-O(6)	2.157(2)	Mn2-O3	2.154(4)0
Mn(2)-O(8)	2.198(2)	Mn2-O6	2.164(4)
Mn(1)-O(1)-Mn(2)	122.16(12)	Mn(1)-O(1)-Mn(2)	124.2(2)
O(1)-Mn(1)-N(2)	171.32(10)	O1-Mn1-N1	167.74(18)
O(5)-Mn(1)-N(1)	168.70(9)	O2-Mn1-N2	169.30(17)
O(3)-Mn(1)-O(7)	172.58(8)	O5-Mn1-O9	170.91(17)
O(1)-Mn(2)-N(4)	170.10(10)	O1-Mn2-N4	169.82(18)
O(4)-Mn(2)-N(3)	169.06(10)	O4-Mn2-N3	168.03(17)
O(6)-Mn(2)-O(8)	173.16(8)	O3-Mn2-O6	164.77(15)
O(7)-Mn(1)-Mn(2)-O(8)	83.8(1)	O9-Mn1-Mn2-O6	–96.3(2)
O(3)-C(26)-C(27)-C(28)	–0.3(4)	O5-C32-C33-C38	–65.1(9)
O(6)-C(34)-C(35)-C(40)	–5.5(4)	O3-C25-C26-C27	35.8(8)

The carboxylate group and the aromatic ring of the benzoate derivative bridge are almost coplanar in compound **1**; the twist angle ω(O-C$_{carb}$-C$_{ar}$-C$_{ar}$) is close to zero. In contrast, a significant twist of the aromatic ring is found in compound **2**, probably due to the steric hindrance between phen ligands and the bromo-substituent, in *ortho* position. The relative disposition of the two coordination octahedra is almost perpendicular, with a torsion angle τ(L-Mn···Mn-L) smaller for compound **1** (83.8º) than for compound **2** (96.3º). Some hydrogen bonds connecting the monodentate ligand and the counter-anion are presents in the crystal

structure of compounds **1** and **2**. For **2**, the net of hydrogen bonds generate a zig-zag chain (Fig S1, S2 and Table S7).

As it was mentioned above, in this kind of compounds, the Mn_{III} ions show an elongated octahedron in the direction of the monodentate ligand; hence, the Jahn-Teller elongation axis should be approximately situated on the O_t-Mn-L direction (z axis). Moreover, there are some rhombic distortion, due to the fact that the Mn-O_b distance is shorter than the Mn-O_c distance and the x axis could be considered in the N_t-Mn-O_b direction (Figure 2). Approximate values of the octahedron axis lengths can be found by addition of Mn–ligand distances: $x = d(Mn–O_b) + d(Mn–N_t)$, $y = d(Mn–O_c) + d(Mn–N_c)$ and $z = d(Mn–O_t) + d(Mn–O_L)$.
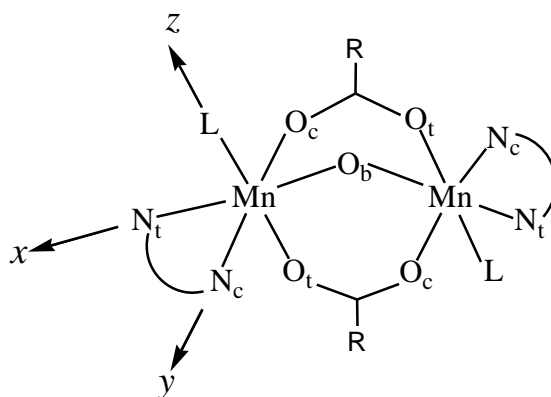
Figure 2. Schematic structure of the dinuclear Mn_{III} complexes with the axes of the octahedron.

Recently, we reported the importance of quantify separately the elongation and the rhombicity of the coordination octahedron for this kind of compounds. The elongation (Δ) and rhombicity (ρ) parameters could be calculated using the following formulae:[9]

$$\Delta = \frac{z - \overline{xy}}{\overline{xy}} \quad \text{and} \quad \rho = \frac{y - x}{x}$$

These parameters are dimensionless and for clarity, it could be expressed in percentage. As it was reported, if $\Delta > \rho$ and both values positives, the octahedron is elongated in the z direction

with small or moderate rhombic distortion.[9] Table 3 summarizes the axis length and the distortion parameters Δ and ρ for compounds **1** and **2**. For both compounds the trend of the length axis is $z > y > x$, as it was observed for analogous compounds. The Δ and ρ values for this kind of systems (with terminal bidentate + monodentate ligand) range between 9.0−15.6% and 3.5−5.4% respectively (average values for the two Mn_{III} ions).[9] The parameters found for compound **1** are in these range and the coordination octahedra is elongated in the monodentate ligand direction.

Table 3. x, y and z axis length, and elongation (Δ) and rhombicity (ρ) parameters for compound **1** and **2** (z axis in the monodentate ligand direction, Figure 2).

		$z\,/\,\text{Å}$	$y\,/\,\text{Å}$	$x\,/\,\text{Å}$	$\Delta\,/\,\%$	$\rho\,/\,\%$
1	Mn1	4.384	4.062	3.885	10.32	4.56
	Mn2	4.355	4.049	3.852	10.24	5.11
					Av. 10.28	4.84
2	Mn1	4.235	4.155	3.864	5.62	7.53
	Mn2	4.318	4.092	3.848	8.77	6.34
					Av. 7.20	Av. 6.94

For compound **2** the anomalous result observed for Mn1, where $\rho > \Delta$, indicates that the axes are not correctly assigned. Moreover, Mn2 shows quite similar values of the elongation and rhombicity parameters, suggesting a great degree of rhombicity or a bad axis assignment. Therefore, for this compound we consider a new set of axis, the z axis being in the Mn-O_b direction and the x axis pointing to the monodentate ligands. The reassignment of the axes and the new values of the distortion parameters are summarized in Table 4. These results confirm that Mn1 shows a compressed octahedron in the direction of the oxo bridge, in agreement with the negative value of Δ. For Mn2 it is clear that shows an important rhombic distortion, but the

magnitude of the distortion parameters is similar with both assignation of the axes. So, the disposition of the Jahn-Teller axis from the structural parameters is ambiguous.

As indicated previously, to the best of our knowledge, there is only another compound of this kind, with bidentate capping ligand and compressed octahedra, reported in the literature. This is the neutral complex [{Mn(N$_3$)(bpy)}$_2$(μ-C$_6$H$_5$COO)$_2$(μ-O)][10,11] (**A**), where both manganese ions are equivalent. In this case, with the same assignation axis than for compound **2**, the distortion parameters Δ and ρ are -7.68 and -1.62 respectively. These parameters are similar to the ones found for Mn1 in compound **2**.

Table 4. x, y and z axis length (x in the monodentate ligand direction and z in the oxo bridge direction), and elongation (Δ) and rhombicity (ρ) parameters for compound **2** and for compound [{Mn(N$_3$)(bpy)}$_2$(μ-C$_6$H$_5$COO)$_2$(μ-O)] (**A**).[10,11]

		x / Å	y / Å	z / Å	Δ / %	ρ / %
2	Mn1	4.235	4.155	3.864	-7.89	-1.89
	Mn2	4.318	4.092	3.848	-8.49	-5.23
					Av. -8.19	Av. -3.56
A	Mn	4.253	4.184	3.895	-7.68	-1.62

Magnetic properties

Magnetic susceptibility data were recorded for compounds **1** and **2** from room temperature to 2 K. For compound **1** the $\chi_M T$ product is ~5.9 cm$_3$ mol$_{-1}$ K at room temperature, which is close to the expected value for two uncoupled Mn$_{III}$ ions (6.0 cm$_3$ mol$_{-1}$ K). The $\chi_M T$ values decrease slightly with the temperature until ~50 K, below this temperature the $\chi_M T$ values

decreases more abruptly on cooling reaching a value of 2.4 cm^3 mol$_{-1}$ K at 2 K (Figure 3). This behavior is indicative of an antiferromagnetic coupling between the Mn$_{III}$ ions. However, the $\chi_M T$ value at low temperature and the shape of the $M/N\mu_\beta$ vs H plot, at 2 K, (Figure 3, inset) suggest the presence of more than one spin state populated at this temperature. Both facts could be explained by the population at low temperatures of excited states with $S \neq 0$ and zero-field splitting (ZFS). Recently it was reported the importance on the disposition of the Jahn-Teller axis and the ZFS parameters of the Mn$_{III}$ ions (D_{Mn} and E_{Mn}) on the magnetic behavior of weak antiferromagnetic dinuclear systems.[9] The fit of the experimental data was performed with the PHI program[33] assuming that the two Mn$_{III}$ ions present the same g, D_{Mn} and E_{Mn} values. Taking in consideration that the Jahn-Teller axes of the coordination octahedra are mostly orthogonal, the Euler angle β was assumed as 90º (-45º for Mn1 and +45º for Mn2). The best fit of $\chi_M T$ and $M/N\mu_\beta$ data was obtained with $J = -1.82$ cm$_{-1}$, $D_{Mn} = -4.07$ cm$_{-1}$ $E_{Mn} = +0.77$ cm$_{-1}$ and $g = 1.99$, with $R_{sus} = 5.3 \times 10_{-5}$ and $R_{mag} = 5.4 \times 10_{-4}$ (values reported using the spin Hamiltonian $H = -JS_1 \cdot S_2$).
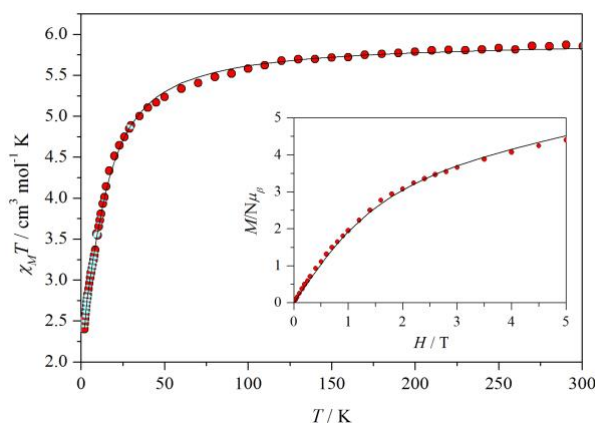
Figure 3. $\chi_M T$ vs. T and $M/N\mu_B$ vs. H (inset) plots for compound **1**. The solid line is the best fit to the experimental data.

For compound **2** the $\chi_M T$ values increases on cooling from ~6.6 cm^3 mol$_{-1}$ K at room temperature to 9.25 cm^3 mol$_{-1}$ K at 17 K. Below this temperature $\chi_M T$ decreases reaching a

value of ~ 7.5 cm$_3$ mol$_{-1}$ K at 2 K. (Figure 4 inset). This behaviour is characteristic of a ferromagnetic coupling. The $\chi_M T$ value expected for a system with a ground spin state $S = 4$ is 10 cm$_3$ mol$_{-1}$ K; the lower values found for the $(\chi_M T)_{max}$ and the decreasing of $\chi_M T$ below this temperature could be explained by the presence of zero-field splitting on the ground state and/or intermolecular antiferromagnetic interactions. As mentioned, this compound shows hydrogen bonds between dinuclear entities, through nitrate anions; thus, intermolecular antiferromagnetic interactions could contribute to the decreases of the $\chi_M T$ values at low temperature.

Magnetization measurements were carried out at six different fields (0.5 — 5 T) in the 1.8 — 6.8 K range. $M/N\mu_B$ versus HT_{-1} plots are shown in Figure 4. The non-superposition of the lines indicates significant zero-field splitting within the ground state.
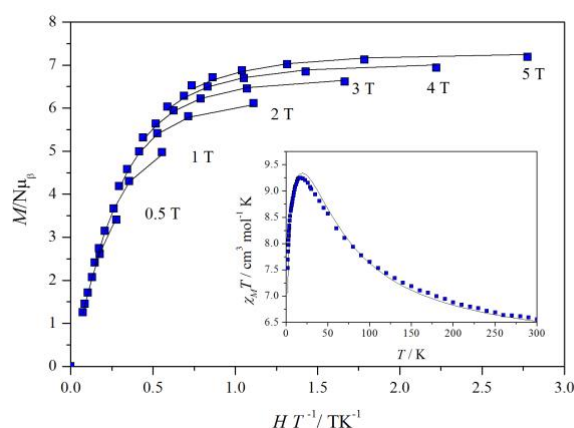
Figure 4. $M/N\mu_B$ vs. HT_{-1} and $\chi_M T$ vs. T (inset) plots for compound **2**. The solid line is the best fit to the experimental data.

The experimental data ($M/N\mu_B$ vs. HT_{-1} and $\chi_M T$ vs. T) were fitted simultaneously with the PHI program.[33] To obtain a good fit was necessary to include the term of intermolecular interactions, that was fixed to $zJ' = –0.015$ cm$_{-1}$. The best fit was obtained with positive D_{Mn} values and negative and smaller E_{Mn} values. Note that the sign of the ZFS parameters is opposite to that found for compound **1** and those reported previously for analogous

compounds.[9] This fact agrees with the compression found in one of the manganese ions. Taking in consideration the different disposition of the Jahn-Teller axis, at least for one of the Mn$_{III}$ ions, several fits were performed with different set of Euler angles. The best fit, considering α = +25º, −25º, β = −40º, +40º and γ = 0º, 0º, lead J = +11.8 cm-1, D_{Mn} = +3.2 cm–1, E_{Mn} = − 0.7 cm–1 and g = 1.98, with R_{sus} = 3.1 × 10–4 and R_{mag} = 4.7 × 10–5 (values reported using the spin Hamiltonian $H = -JS_1 \cdot S_2$). However, similar graphs could be obtained with α = +15º, −15º, β = −40º, +40º and γ = 0º, 0º lead J = +12.0 cm-1, D_{Mn} = +3.8 cm–1, E_{Mn} = −0.6 cm–1 and g = 1.98.

It has been previously reported that in Mn$_{III}$ dinuclear systems bridged by (μ-O)(μ-RCOO)$_2$, the μ-O bridge facilitates the superexchange coupling through an out of plane π interaction, while the carboxylate bridge impedes the magnetic coupling reducing the antiferromagnetic interaction, showing a countercomplementary effect.[34] A qualitative analysis of the exchange pathways through the μ-O bridge can be done for both complexes. For each Mn$_{III}$ ion there are four singly-occupied orbitals. Depending on their delocalization and overlap with the ligand orbitals they will contribute differently to the coupling.

Figure 5 shows the disposition axis for both compounds. The qualitative analysis of the exchange pathways shows similar π interactions through the μ-O bridge in both complexes. Although there is a different orientation of the axis the most important antiferromagnetic contribution is common in both complexes, for **1** it is the xz(Mn1)/xy(Mn2) interaction while for **2** it is the xz(Mn1)/yz(Mn2) interaction. The other common π interaction, in the MnOMn plane, is the xy(Mn1)/xz(Mn2) interaction for **1** and yz(Mn1)/xz(Mn2) interaction for **2**, which is sensitive to the Mn-O$_b$-Mn angle. There are however three interactions that are present only in **1** due to the different arrangements of the magnetic axis, the z_2(Mn1)/z_2(Mn2) interaction, which will depend on the angle, the z_2(Mn1)/xz(Mn2) and the xy(Mn1)/z_2(Mn2) interactions. The three of them are expected to be antiferromagnetic.
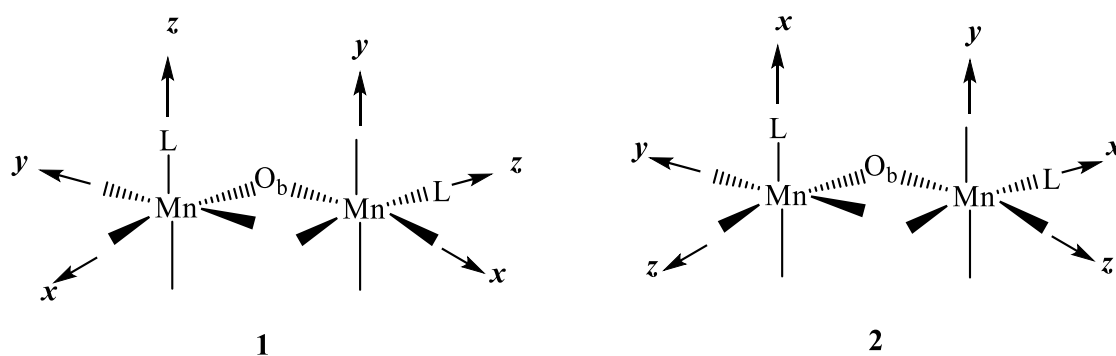
Figure 5. Schematic representation of the axis disposition for both compounds.

This qualitative analysis shows that complex **1** have more antiferromagnetic contributions, from the singly occupied z_2 orbital, than compound **2**, due to the different arrangement of the magnetic axis. However, it has been previously seen that the magnetic interaction in these complexes is very sensitive to very small structure variations as most of these contributions are geometry dependent.

In a previous work we reported some magneto-structural correlation for this kind of dinuclear compounds [9] As it was indicated, most of them show elongated octahedra with some rhombic distortion. The exceptions are compound **A** (reported in table 4)[11] and compound **2** that show compressed octahedra. For the compounds with elongated/rhombic distortion, those with the most elongated octahedra show an average value of $\Delta = 15{,}6\%$ and $\rho = 3.5\%$ ($\Delta/\rho = 4.5$) and antiferromagnetic behaviour.[9] In the other extreme, the compound with a major degree of rhombicity shows $\Delta = 9.0\%$ and $\rho = 5.4\%$ ($\Delta/\rho = 1.7$) and ferromagnetic behaviour.[9,32] Compound **1**, with $\Delta = 10.3\%$ and $\rho = 4.8\%$ ($\Delta/\rho = 2.1$) shows weak antiferromagnetic behavior, as expected for this structural distortion. Moreover, the correlation $|E_{Mn}/D_{Mn}|$ vs ρ reported previously ($|E_{Mn}/D_{Mn}| = 0.06 + 0.03\ \rho$, where ρ is in percentage)[9] fits well for compound **1**. In basis to the ρ value calculated from the structural parameters, the expected $|E_{Mn}/D_{Mn}|$ value should be 0.20 that is the same relationship found by the fit of the magnetic data.

The three structural parameters that modulate the magnetic interaction are the elongation parameter Δ, the twist of the phenyl ring towards the carboxylate group (ω) and the relative disposition of the coordination octahedra (τ). Compound **1** shows a moderate Δ value, a non-relevant ω angle, due to the substituent in *para* position, and a small τ angle (83.8º). This angle for this kind of compounds range from 73.3º to 120;[9,32] in general, compounds with small τ angle show antiferromagnetic behavior. So, the weak magnetic behavior can be explained with the competition of both factors: the significant degree of rhombicity ($\Delta/\rho = 2.1$) that promote the ferromagnetic behavior and the small τ angle that works in the opposite direction.

Theoretical calculations

With the aim to found a relationship between the structural parameters and the magnetic behaviour of **1** and **2**, two kinds of calculations were carried out. For the calculation of the ZFS parameter a multiconfigurational methodology was employed (CASSCF+RASSI), which has been used satisfactorily to obtain ZFS parameters in other Mn_{III} complexes.[13] Each Mn_{III} was calculated independently, replacing the other Mn_{III} ion by Ga_{III} ion and preserving the structural data of the whole complex. The magnetic coupling constants (J) were obtained using a procedure previously described in literature.[21–23] Using DFT calculations with Gaussian basis set and B3LYP functional the J value was obtained from the energy difference between the high spin ($S_T = 4$) and low spin configurations ($S_T = 0$), see computational details section. The results of these calculations are collected in Table 5 together with the values obtained from the fit of the experimental data.

Table 5. Magnetic coupling constant (J) and ZFS parameters for the Mn_{III} ions obtained from the fit of the experimental data. Calculated J values using DFT and the B3LYP functional and calculated ZFS parameters at CASSCF+RASSI level. ($H = -J\,S_1 \cdot S_2$).

| | From the fit of the experimental data | | | B3LYP | CASSCF + RASSI | |
	J (cm^{-1})	D (cm^{-1})	E (cm^{-1})	J (cm^{-1})	D_1/D_2 (cm^{-1})	$|E_1|/|E_2|$ (cm^{-1})
1	−1.8	−4.1	+0.8	−3.14	−3.17 −3.12	0.89 0.94
2	+11.8	+3.2	−0.7	+12.89	+3.53 +3.35	0.66 0.83

The calculated ZFS parameters of each ion in these compounds corroborate the values obtained from the experimental fit, giving a $D_{Mn} < 0$ for the elongated compound **1** and a $D_{Mn} > 0$ for the compressed compound **2**. It is worth noting, that for compound **2**, the D_{Mn} of both ions is of positive sign, indicative of a compressed octahedron. Moreover, the $|E/D|$ ratio for Mn1 is 0.19 while for Mn2 0.25 in agreement with the major rhombicity found for Mn2.

It was previously reported that the qualitative sign and magnitude of the D value of the single ion in mononuclear first row transition metal compounds can be predicted based in the coordination and electronic structure of the metal center.[35] The D_{Mn} value is calculated from the elements of the diagonalized $\boldsymbol{D}$ tensor ($\boldsymbol{D} = D_{zz} - (D_{xx} + D_{yy})/2$). Looking at that equation is possible to obtain the sign of the D_{Mn} value, as it will depend on the relative value of the D_{zz}

and $(D_{xx} + D_{yy})/2$ terms. If the former term is larger the D_{Mn} value is negative while in the opposite case ($|(D_{xx} + D_{yy})/2| > |D_{zz}|$) the D_{Mn} value is positive. The analysis of the components of the tensor, D_{ii}, showed that the principal contributions D_{zz} came from the excitation between pair of orbitals with the same $|m_l|$ value, while the principal contributions to D_{xx} and D_{yy} came from the excitation between pair of orbitals with m_l changes of ±1, and that the D_{ii} value is inversely proportional to the energy difference between the orbitals involved in the excitation.

The structural distortion due to the Jahn-Teller effect in the studied complexes will affect to the splitting of the 3d orbitals (Figure 6) and consequently to the D_{Mn} value. For an elongated octahedron, as in compound **1**, the empty orbital is the d_{x2-y2} while for compound **2** should be the d_{z2}. For **1**, the first excitation involves the d_{xy} and d_{x2-y2} orbitals, with the same m_l value, giving to a larger D_{zz} contribution and consequently a negative D_{Mn} value. However, for **2**, the first excitations involve the d_{xz} or d_{yz} and d_{z2} orbitals, with a difference in m_l value of ±1, giving to a larger D_{xx} and D_{yy} contributions and consequently a positive D_{Mn} value. In both cases the first excitation is expected to involve large excitation energies from the nonbonding (d_{xy} or d_{xz} or d_{yz}) to the antibonding ($d_{x2−y2}$ or d_{z2}) orbitals giving to relative small D_{Mn} values, although the relative energy of those orbitals can change depending on the coordinated ligands and the distortion from the octahedron. The calculated and experimentally obtained D_{Mn} values are in concordance with this qualitative model, with relative small D_{Mn} values (around 3 cm-1) being negative for **1** and positive for **2**.

Figure 6. Schematic orbital diagram for d_4 metal ion in octahedral geometry depending on the distortion, elongated *vs* compressed.

In addition, it is expected that the axis will show different orientation because for compound **1** the elongation z axis is approximatively pointing to the monodentate ligand, while for compound **2** the compression z axis points to the oxo bridge. Figure 7 shows the orientation of the D_{ii} components of the **D** tensor for **1** and **2**. It can be observed that the anisotropy tensors are almost aligned along the metal-ligand bonds. For **1**, the D_{zz} components are aligned with the Mn-monodentate ligand bonds while the D_{xx} are aligned with the Mn-oxo bonds. However, for **2** the D_{zz} components are aligned with the Mn-oxo bonds and the D_{xx} are aligned with the Mn-monodentate ligand bonds.

Figure 7. Principal axes of the D_{ii} components of the D tensor for **1** (left) and **2** (right). D_{xx}, D_{yy} and D_{zz} are represented with blue, green and yellow arrows respectively. Manganese, bromide, oxygen, nitrogen and carbon atoms are represented in pink, yellow, red, blue and grey respectively.

These results indicate that in compound **1** both Mn$_{III}$ ions have uniaxial anisotropy with the easy axis oriented almost in the Mn-monodentate ligand bonds. In the case of compound **2**, both Mn$_{III}$ ions are easy plane with the easy plane perpendicular to the to the Mn-oxo bonds. These results corroborate that the geometry in Mn2 in compound **2** can be better assigned as compressed octahedron with major rhombicity, second assignment performed in the description of structures (x in the monodentate ligand direction and z in the oxo bridge direction). The difference in the orientation of the axes between compounds **1** and **2** will affect to different coupling pathways through the bridging ligands.

The magnitude and sign of the J values obtained from DFT calculations agrees with that found from the fit of the experimental data, corroborating the obtained exchange coupling

constants, antiferromagnetic for **1**, with elongated geometry, and ferromagnetic for **2**, with compressed geometry. It has been previously observed that the exchange coupling constants are very sensible to small changes in the geometry, and in this case, it is particularly sensitive to the angle between both Mn ions through the oxo bridging ligand due to the contribution of the μ-O bridge to the exchange pathways. To gain more insight into it, we have modified the Mn-O_b-Mn angle (α) moving the oxo bridge (O_b) atom along the axis formed by the O atom and the middle point between both Mn ions, the pseudo C_2 axis of the Mn_2O core (dotted red line in Figure 8). In this kind of dinuclear compounds, α usually varies between 120 and 125°, been this range the selected one for the study. Moreover, the effect of the elongation or compression along the monodentate ligand direction and along the O_{bridge}-N_{trans} directions have been analyzed (Figure 8).
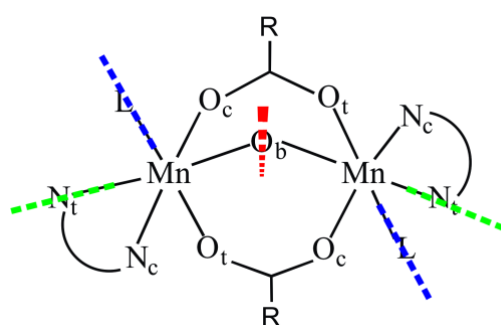
Figure 8. Schematic structure of the dinuclear Mn$_{III}$ complexes showing the geometric variations performed for the creation of the different models. The change in α has been done moving O_b along the pseudo C_2 axis of the Mn_2O core (red dotted line), the variation of d_{Mn-L} has been performed moving the monodentate ligand along the Mn-L bond (blue dotted lines), and the change of d_{Mn-Nt} has been achieved moving the phen ligand along the Mn-N_t bond (green dotted lines).

Figure 9 shows the dependence of the calculated J value with the variation of the Mn-O_b-Mn angle (see also Tables S1 and S2). Although **1** is antiferromagnetic having a smaller angle and **2** is ferromagnetic with a larger one in both cases the same tendency is observed, when α is increased the magnetic coupling becomes more antiferromagnetic (or less ferromagnetic) and when it is decreased the magnetic behavior becomes more ferromagnetic. In fact, for the models derived of compound **1** when α is smaller than 121° a ferromagnetic coupling is obtained.
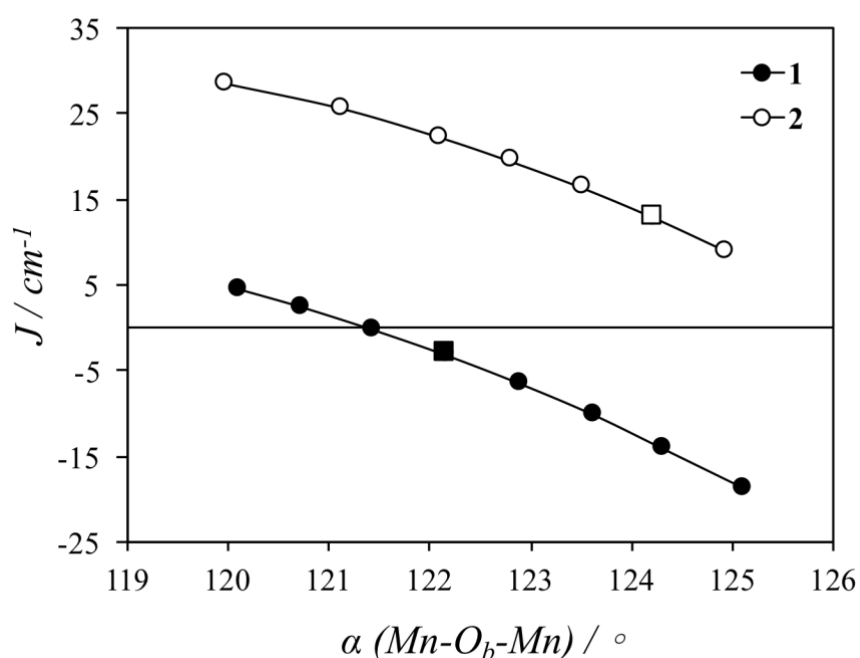
Figure 9. Dependence of the calculated J value with the Mn-O_b-Mn angle in the model. The square represents the calculated J value for the experimental geometry.

However, although the change in the Mn-O_b-Mn angle clearly affects the magnetic behavior and the observed tendency is the same for the models derived of both complexes, models derived from compound **2** shows larger ferromagnetic behaviour. As described before in the qualitative analysis of the exchange pathways it can be due to the presence of three extra antiferromagnetic interactions in **1** through the μ-O bridge. However, it can also be related to

the different geometry (elongation *vs* compression) and distortion from the ideal octahedron. To better understand how that will affect the exchange coupling two different models have been created changing the distance between the Mn ions and monodentate ligand or the phen ligand (Figure 8). These to ligands have been chosen because they are not bridging ligands between both Mn ions, so we are not altering the coupling pathway, but the modification of these Mn-ligand distances allows us to alter the elongation/compression and rhombocity of the Mn ions.

The Mn-monodentate ligand bond distance (d_{Mn-L}) in this type of compounds usually varies between 2.10 and 2.48 Å, being for the complexes studied here between 2.13 and 2.23 Å. We have chosen to vary this distance between 2.1 and 2.3 Å (see table S3 and S4). An increase in d_{Mn-L} will increase the absolute value of the elongation parameter (Δ) while the rhombocity parameter (ρ) will be constant for **1** but not for **2** because of the different orientation of the axes. As it was explained in the precedent section, the Δ parameter represents the elongation ($\Delta > 0$) or compression ($\Delta < 0$) of the octahedra and major $\left| \Delta \right|$ values means that the coordination octahedra is further from the ideal geometry, independently of the orientation axes. As Figure 10 shows, in both cases when d_{Mn-L} increases ($\left| \Delta \right|$ increases) the coupling becomes more antiferromagnetic (less ferromagnetic). In the case of **1**, for distances below 2.13 Å the J becomes ferromagnetic.

In the case of the phen ligand, we have modified the distance between the Mn ions and the N in trans to the oxo ligand (d_{Mn-Nt}), dotted green lines in Figure 8. We have kept the phen ligand unaltered, so when d_{Mn-Nt} changes it translates all the phen ligand and consequently it modifies the distance between the Mn and the cis N atom. Typical Mn-N distances oscillate between 2.02 and 2.1 Å, interval that we have chosen to vary d_{Mn-Nt} (see Table S5 and S6). The increase on this distance decreases the $\left| \Delta \right|$ and $\left| \rho \right|$ parameters. As shown in figure 10, the

decrease of d_{Mn-Nt} ($|\Delta|$ increase) makes the coupling more antiferromagnetic (less ferromagnetic).
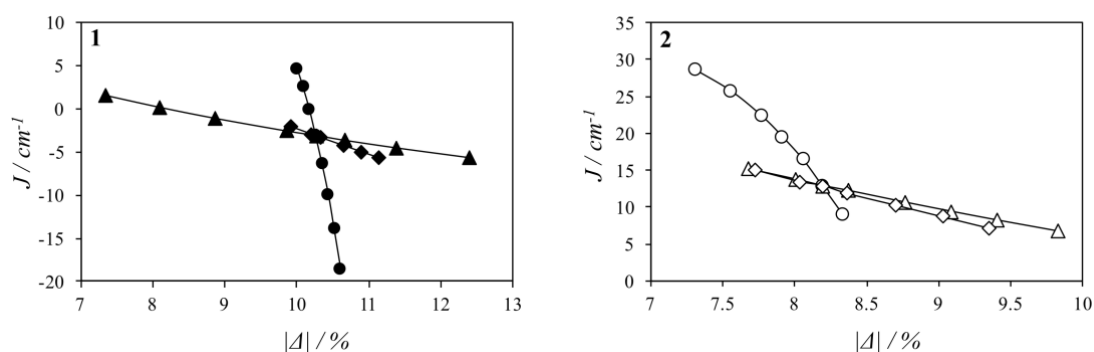
Figure 10. Dependence of the calculated J value with the average Δ parameter, in absolute value, for the different models created for compounds **1** (left) and **2** (right). Circles represent when the Mn-O_b-Mn angle (α) is changed, triangles represent the model where the Mn-monodentate ligand distance (d_{Mn-L}) is modified and diamonds represent the model for which the Mn-N_{trans} distance (d_{Mn-Nt}) is modified.

If we compare the three models we see that the structural parameter that affects more the exchange coupling constant is α, the Mn-O_b-Mn angle, which is expected because the O atom is bridging both Mn atoms and we are directly altering the coupling pathway. In all the cases the increase in the $|\Delta|$ parameter makes the coupling more antiferromagnetic (less ferromagnetic). As explained before, the Δ parameter represents the elongation ($\Delta > 0$) or compression ($\Delta < 0$) of the octahedra and a larger $|\Delta|$ value indicates a more elongated or compressed geometry, so in both cases the coupling is more antiferromagnetic when the Mn coordination environment is more distorted, more elongated for compound **1** and more compressed for **2**. The modification of the Mn-ligand bond distances, d_{Mn-L} or d_{Mn-Nt}, gives to a smaller variation of the magnetic coupling and very similar trends in all the cases, even when the variation in the rhombocity parameter (ρ) are different in each case. It indicates that the

elongation/compression is still affecting the magnetic coupling, even when the geometry of the ligands involved in the coupling pathway is unaltered, and the larger importance of the Δ parameter in the coupling constant in comparison with the ρ parameter. Moreover, it is important to notice that for compound **1**, all the models considered are should be described with the same axis assignment that in **1** (z axis in the Mn-L direction). For the models derived of compound **2**, the axis assignment of **2** is correct for all of them, except for the model with the largest Mn-L distance (model **2-L7**) where the Δ/ρ ration is greater for z in the Mn-L direction than in the Mn-O$_b$ direction (Tables S8-S11).

CONCLUSIONS

Two dinuclear Mn$_{III}$ compounds with 4-methilbenzoato (**1**) and 2-Bromobenzoato (**2**) bridges and different counteranion (ClO$_4^-$ for **1** and NO$_3^-$ for **2**) have been obtained in a crystalline form. Their structural data reveals significant differences in the shape of the coordination octahedron around the Mn$_{III}$ ions in both compounds and different disposition of the Jahn-Teller axis. For **1** the elongation axis point to the mondentate ligand, while for **2** the coordination octahedra are compressed in the oxo-bridge direction. These factors affects to the magnetic interaction and the zero-field splitting parameters of the Mn$_{III}$ ions (D_{Mn} and E_{Mn}). Compound **1** shows a ground state $S = 0$ and $D_{Mn} < 0$, while compound **2** shows a ground sate $S = 4$ and $D_{Mn} > 0$.

Theoretical calculations corroborate the experimental findings. In the case of Mn2 in compound **2**, it also shows larger $|E/D|$ ratio, which agrees with the major rhombicity found experimentally, and helps in the correct assignment of the axis. The different exchange coupling observed for these compounds was also well reproduced. In addition, magneto-structural correlations show that the most important structural parameter studied is, as expected, the Mn-O$_b$-Mn angle. Moreover, they also show that the increase of the

$|\Delta|$ parameter gives more antiferromagnetic character to the coupling and that the effect of the rhombocity parameter (ρ) is smaller.

ASSOCIATED CONTENT

Supporting Information. Detail of the models used for the calculations are listed in Tables S1-S6. Figures S1 and S2, and Table 7 show information about the hydrogen bonds presents in the crystal structure of **1** and **2**. X-ray crystallographic files in CIF format for the structure determination of **1** (++++) and **2** (++++). "This material is available free of charge via the Internet at http://pubs.acs.org."

AUTHOR INFORMATION

Corresponding Author

* Montserrat Corbella Cordomí, e-mail: montse.corbella@gmail.com.

* Silvia Gómez Coca, e-mail :

Present Addresses

† Department of Chemistry, King's College London, London SE1 1DB, United Kingdom

REFERENCES

(1)   Hotzelmann, R.; Wieghardt, K. E.; Florke, U.; Haupt, H. J.; Weatherburn, D. C.; Bonvoisin, J.; Blondin, G.; Girerd, J.-J. J. Spin Exchange Coupling in Asymmetric Heterodinuclear Complexes Containing the Mu-Oxo-Bis(Mu-Acetato)Dimetal Core. *J. Am. Chem. Soc.* **1992**, *114* (5), 1681–1696 DOI: 10.1021/ja00031a023.

(2)   Corbella, M.; Costa, R.; Ribas, J.; Fries, P. H.; Latour, J.-M.; Ohrstrom, L.; Solans, X.; Rodriguez, V. Structural and Magnetization Studies of a New (µ-Oxo)bis(µ-carboxylato)dimanganese(III) Complex with a Terminal Hydroxo Ligand. *Inorg. Chem.* **1996**, *35* (7), 1857–1865 DOI: 10.1021/ic950930x.

(3)   Fernández, G.; Corbella, M.; Alfonso, M.; Stoeckli-Evans, H.; Castro, I. A Comparative XAS and X-Ray Diffraction Study of New Binuclear Mn(III) Complexes with Catalase Activity. Indirect Effect of the Counteranion on Magnetic Properties. *Inorg. Chem.* **2004**, *43* (21), 6684–6698 DOI: 10.1021/ic0348897.

(4)   Gómez, V.; Corbella, M.; Roubeau, O.; Teat, S. J. Magneto-Structural Correlations in Dinuclear Mn(iii) Compounds with Formula [{Mn(L)(NN)}(µ-O)(µ-2-RC6H4COO)2{Mn(L′)(NN)}]n+. *Dalt. Trans.* **2011**, *40* (44), 11968 DOI: 10.1039/c1dt11242b.

(5)   Corbella, M.; Gómez, V.; Garcia, B.; Rodriguez, E.; Albela, B.; Maestro, M. a. Synthesis, Crystal Structure and Magnetic Properties of New Dinuclear Mn(III) Compounds with 4-ClC6H4COO and 4-BrC6H4COO Bridges. *Inorganica Chim. Acta* **2011**, *376* (1), 456–462 DOI: 10.1016/j.ica.2011.07.016.

(6)   Fernández, G.; Corbella, M.; Aullón, G.; Maestro, M. a.; Mahía, J. New Dinuclear MnIII Compounds with 2-MeC6H 4COO and 2-FC6H4COO Bridges - Effect of Terminal Monodentate Ligands (H2O, ClO4- and NO3-) on the Magnetic Properties. *Eur. J. Inorg. Chem.* **2007**, *3* (9), 1285–1296 DOI: 10.1002/ejic.200600708.

(7)   Gómez, V.; Corbella, M.; Aullón, G. Two Temperature-Independent Spinomers of the Dinuclear mn(III) Compound [{Mn(H2O)(phen)}2(µ-2-ClC6H 4COO)2(µ-O)](ClO4)2. *Inorg. Chem.* **2010**, *49* (4), 1471–1480 DOI: 10.1021/ic901719t.

(8)   Gómez, V.; Corbella, M.; Mautner, F. a.; Roubeau, O.; Teat, S. J.; Font-Bardia, M.; Calvet, T. Manganese Compounds with Phthalate and Terephthalate Ligands: Synthesis, Crystal Structure, Magnetic Properties and Catalase Activity. *Polyhedron* **2012**, *45* (1), 185–199 DOI: 10.1016/j.poly.2012.07.036.

(9)   Escriche-Tur, L.; Font-Bardia, M.; Albela, B.; Corbella, M. New Insights into the Comprehension of the Magnetic Properties of Dinuclear MnIII Compounds with the General Formula [{MnL(NN)}2([small Mu]-O)([small Mu]-N-RC6H4COO)2]X2. *Dalt. Trans.* **2016**, *45* (29), 11753–11764 DOI: 10.1039/C6DT01097K.

(10)   J. B. Vincent, K. Folting, J. C. Huffman, and G. C. Dinuclear Manganese Oxide Complexes as Models for Manganese Catalase. *Biochem. Soc. Trans.* **1988**, *16*, 822–823.

(11)   Vincent, J. B.; Tsai, H. L.; Blackman, A. G.; Wang, S.; Boyd, P. D. W.; Folting, K.; Huffman, J. C.; Lobkovsky, E. B.; Hendrickson, D. N.; Christou, G. Models of the Manganese Catalase Enzymes. Dinuclear manganese(III) Complexes with the [Mn2(.mu.-O)(.mu.-O2CR)2]2+ Core and Terminal Monodentate Ligands: Preparation and Properties of [Mn2O(O2CR)2X2(bpy)2] (X = Chloride, Azide, Water). *J. Am. Chem. Soc.* **1993**, *115* (26), 12353–12361 DOI: 10.1021/ja00079a016.

(12)   Corbella, M.; Fernandez, G.; Gonzalez, P.; Maestro, M.; Font-Bardia, M.; Stoeckli-Evans, H. Dinuclear MnIII Compounds [{Mn(bpy)(H2O)}2(mu-4-RC6H4COO)2(mu-

O)](NO3)2 (R = Me, F, CF3, MeO, tBu): Effect of the R Group on the Magnetic Properties and the Catalase Activity. *Eur. J. Inorg. Chem.* **2012**, *2* (13), 2203–2212 DOI: 10.1002/ejic.201101433.

(13) Duboc, C. Determination and Prediction of the Magnetic Anisotropy of Mn Ions. *Chem. Soc. Rev.* **2016**, *248*, 757–815 DOI: 10.1039/C5CS00898K.

(14) Duboc, C.; Ganyushin, D.; Sivalingam, K.; Collomb, M.-N.; Neese, F. Systematic Theoretical Study of the Zero-Field Splitting in Coordination Complexes of Mn(III). Density Functional Theory versus Multireference Wave Function Approaches. *J. Phys. Chem. A* **2010**, *114* (39), 10750–10758 DOI: 10.1021/jp107823s.

(15) Retegan, M.; Collomb, M.-N.; Neese, F.; Duboc, C. A Combined High-Field EPR and Quantum Chemical Study on a Weakly Ferromagnetically Coupled Dinuclear Mn(iii) Complex. A Complete Analysis of the EPR Spectrum beyond the Strong Coupling Limit. *Phys. Chem. Chem. Phys.* **2013**, *15* (1), 223–234 DOI: 10.1039/C2CP42955A.

(16) Sala, T.; Sargent, M. V. Tetrabutylammonium Permanganate: An Efficient Oxidant for Organic Substrates. *Journal of the Chemical Society, Chemical Communications*. 1978, p 253.

(17) Sheldrick, G. . SHELXS97, Program for the Solution of Crystal Structures. *A short Hist. SHELX* **2008**, *64*, 112–122.

(18) Aquilante, F.; De Vico, L.; Ferre, N.; Ghigo, G.; Malmqvist, P.-A.; Neogrady, P.; Pedersen, T. B.; Pitonak, M.; Reiher, M.; Roos, B. O.; Serrano-Andres, L.; Urban, M.; Veryazov, V.; Lindh, R. MOLCAS 7: The next Generation. *J. Comput. Chem.* **2010**, *31* (1), 224–247 DOI: 10.1002/jcc.21318.

(19) Maurice, R.; Guihéry, N.; Bastardis, R.; De Graaf, C. Rigorous Extraction of the Anisotropic Multispin Hamiltonian in Bimetallic Complexes from the Exact Electronic Hamiltonian. *J. Chem. Theory Comput.* **2010**, *6* (1), 55–65 DOI: 10.1021/ct900473u.

(20) Chibotaru, L. F.; Ungur, L. No Title. *J. Chem. Phys.* **2012**, *137*.

(21) Ruiz, E.; Alemany, P.; Alvarez, S.; Cano, J. Toward the Prediction of Magnetic Coupling in Molecular Systems: Hydroxo-and Alkoxo-Bridged Cu (Ii) Binuclear Complexes. *J. Am. Chem. Soc* **1997**, *7863* (Ii), 1297–1303 DOI: 10.1021/ja961199b.

(22) Ruiz, E.; Cano, J.; Alvarez, S. Density Functional Study of Exchange Coupling Constants in Single-Molecule Magnets: The Fe8 Complex. *Chemistry* **2005**, *11* (16), 4767–4771 DOI: 10.1002/chem.200500041.

(23) Ruiz, E. Theoretical Study of the Exchange Coupling in Large Polynuclear Transition Metal Complexes Using DFT Methods. *Struct. Bond.* **2004**, *113*, 71–102 DOI: 10.1007/b97942.

(24) Frisch, M. J.; Trucks, G. W.; Schlegel, H. B.; Scuseria, G. E.; Robb, M. A.; Cheeseman, J. R.; Scalmani, G.; Barone, V.; Mennucci, B.; Petersson, G. A.; Nakatsuji, H.; Caricato, M.; Li, X.; Hratchian, H. P.; Izmaylov, A. F.; Bloino, J.; Zheng, G.; Sonnenberg, J. L.; Hada, M.; Ehara, M.; Toyota, K.; Fukuda, R.; Hasegawa, J.; Ishida, M.; Nakajima, T.; Honda, Y.; Kitao, O.; Nakai, H.; Vreven, T.; Montgomery Jr., J. A.; Peralta, J. E.; Ogliaro, F.; Bearpark, M.; Heyd, J. J.; Brothers, E.; Kudin, K. N.; Staroverov, V. N.; Kobayashi, R.; Normand, J.; Raghavachari, K.; Rendell, A.; Burant, J. C.; Iyengar, S. S.; Tomasi, J.; Cossi, M.; Rega, N.; Millam, J. M.; Klene, M.; Knox, J. E.; Cross, J. B.; Bakken, V.; Adamo, C.; Jaramillo, J.; Gomperts, R.; Stratmann, R. E.; Yazyev, O.; Austin, A. J.; Cammi, R.; Pomelli, C.; Ochterski, J. W.; Martin, R. L.; Morokuma, K.; Zakrzewski, V. G.; Voth, G. A.; Salvador, P.; Dannenberg, J. J.; Dapprich, S.; Daniels,

A. D.; Farkas, Ö.; Foresman, J. B.; Ortiz, J. V; Cioslowski, J.; Fox, D. J. Gaussian 09, Revision A.02. *Gaussian Inc Wallingford CT*. 2009, p Wallingford CT.

(25)   Becke, A. D. Density-Functional thermochemistry.III. The Role of Exact Exchange. *J. Chem. Phys.* **1993**, *98* (7), 5648 DOI: 10.1063/1.464913.

(26)   Schäfer, A.; Huber, C.; Ahlrichs, R. Fully Optimized Contracted Gaussian Basis Sets of Triple Zeta Valence Quality for Atoms Li to Kr. *J. Chem. Phys.* **1994**, *100* (8), 5829.

(27)   Schrödinger, I. Jaguar 6.0 Ed. Portland 2007.

(28)   Vacek, G.; Perry, J. K.; Langlois, J.-M. Advanced Initial-Guess Algorithm for Self-Consistent-Field Calculations on Organometallic Systems. *Chem. Phys. Lett.* **1999**, *310* (1–2), 189–194 DOI: 10.1016/S0009-2614(99)00722-8.

(29)   Deacon, G. Relationships between the Carbon-Oxygen Stretching Frequencies of Carboxylato Complexes and the Type of Carboxylate Coordination. *Coord. Chem. Rev.* **1980**, *33* (3), 227–250 DOI: 10.1016/S0010-8545(00)80455-5.

(30)   Gómez, V.; Corbella, M.; Aullón, G. Two Temperature-Independent Spinomers of the Dinuclear mn(III) Compound [{Mn(H2O)(phen)}2(μ-2-ClC6H 4COO)2(μ-O)](ClO4)2. *Inorg. Chem.* **2010**, *49* (4), 1471–1480 DOI: 10.1021/ic901719t.

(31)   Chen, C.; Zhu, H.; Huang, D.; Wen, T.; Liu, Q.; Liao, D.; Cui, J. Syntheses, Structures and Magnetic Properties of Mono- and Di-Manganese Inclusion Compounds. *Inorganica Chim. Acta* **2001**, *320* (1–2), 159–166 DOI: 10.1016/S0020-1693(01)00489-3.

(32)   Gómez, V.; Corbella, M. Catalase Activity of Dinuclear Mn III Compounds with Chlorobenzoato Bridges. *Eur. J. Inorg. Chem.* **2012**, *2* (19), 3147–3155 DOI: 10.1002/ejic.201200143.

(33)   Chilton, N. F.; Anderson, R. P.; Turner, L. D.; Soncini, A.; Murray, K. S. PHI: A Powerful New Program for the Analysis of Anisotropic Monomeric and Exchange-Coupled Polynuclear D- and F-Block Complexes. *J. Comput. Chem.* **2013**, *34* (13), 1164–1175 DOI: 10.1002/jcc.23234.

(34)   Pantazis, D. A.; Krewald, V.; Orio, M.; Neese, F. Theoretical Magnetochemistry of Dinuclear Manganese Complexes: Broken Symmetry Density Functional Theory Investigation on the Influence of Bridging Motifs on Structure and Magnetism. *Dalt. Trans.* **2010**, *39* (20), 4959–4967 DOI: 10.1039/C001286F.

(35)   Gomez-Coca, S.; Cremades, E.; Aliaga-Alcalde, N.; Ruiz, E. Mononuclear Single-Molecule Magnets: Tailoring the Magnetic Anisotropy of First-Row Transition-Metal Complexes. *J. Am. Chem. Soc.* **2013**, *135* (18), 7010–7018 DOI: 10.1021/ja4015138.

TOC GRAPHIC AND SYNOPSIS

Different magnetic behavior for two similar Mn$_{III}$ dinuclear compounds with 4-Me or 2-Brbenzoato bridges. The orientation of the Jahn-Teller axis is crucial for the magnetic interaction and the sign of the ZFS parameters.

Two kind of distortions

Compresion in the O_b direction
$S = 4$
$D_{Mn} > 0$

Elongation in the L direction $S = 0$
$D_{Mn} < 0$